Eur. Phys. J. C (2024) 84:246
https://doi.org/10.1140/epjc/s10052-024-12569-0

THE EUROPEAN PHYSICAL JOURNAL C

Regular Article - Theoretical Physics

Unitarity bounds on the massive spin-2 particle explanation of muon $g-2$ anomaly

Da Huang[1,2,3,a], **Chao-Qiang Geng**[2,3,b], **Jiajun Wu**[2,3,4,c]

[1] National Astronomical Observatories, Chinese Academy of Sciences, Beijing 100012, China
[2] School of Fundamental Physics and Mathematical Sciences, Hangzhou Institute for Advanced Study, UCAS, Hangzhou 310024, China
[3] International Centre for Theoretical Physics Asia-Pacific, Beijing/Hangzhou, China
[4] CAS Key Laboratory of Theoretical Physics, Institute of Theoretical Physics, Chinese Academy of Sciences, Beijing 100190, China

Received: 8 June 2023 / Accepted: 18 February 2024

Abstract Motivated by the long-standing discrepancy between the Standard Model prediction and the experimental measurement of the muon magnetic dipole moment, we have recently proposed to interpret this muon $g-2$ anomaly in terms of the loop effect induced by a new massive spin-2 field G. In the present paper, we investigate the unitarity bounds on this scenario. We calculate the s-wave projected amplitudes for two-body elastic scatterings of charged leptons and photons mediated by G at high energies for all possible initial and final helicity states. By imposing the condition of the perturbative unitarity, we obtain the analytic constraints on the charged-lepton-G and photon-G couplings. We then apply our results to constrain the parameter space relevant to the explanation of the muon $g-2$ anomaly.

1 Introduction

One of the greatest puzzles in the Standard Model (SM) is the discrepancy between the SM theoretical prediction and experimental data on the muon magnetic dipole moment $(g-2)_\mu$ [1], which is regarded as a hint towards new physics beyond the SM (BSM). Currently, by combining the data from Brookhaven [2] and Fermilab [3], the muon $g-2$ anomaly is given by

$$\Delta a_\mu = a_\mu^{\rm exp} - a_\mu^{\rm SM} = (25.1 \pm 5.9) \times 10^{-10}, \quad (1)$$

where the latest SM calculation leads to $a_\mu^{\rm SM} = (116591810 \pm 43) \times 10^{-11}$ [4–24] (see e.g. Ref. [25] for a recent review and references therein). Already, many BSM models have been proposed in order to resolve this muon $g-2$ discrepancy (for a recent review see e.g. [26] and references therein).

In Ref. [27], we have demonstrated that the muon $g-2$ anomaly can be explained by the one-loop effects induced by a new spin-2 particle G, which can be identified as the first Kaluza–Klein (KK) graviton in the generalized Randall–Sundrum (RS) model [28–44]. By calculating all relevant one-loop Feynman diagrams, we have obtained the analytic expression of the leading-order G-induced contribution to the muon $g-2$. Although the loop integrals are highly power-law divergent, we applied the Loop Regularization method [45,46] to maintain both the gauge invariance of the quantum electrodynamics and the correct divergence structure of loop integrals. As a result, the divergent integrals become well-behaved analytical expressions depending on the UV cutoff scale. With a given value of the UV cutoff, the theory becomes predictable. We have also taken into account theoretical bounds from perturbativity and experimental constraints from LEP-II and LHC. It turns out that there is a large amount of allowed parameter space to explain the muon $g-2$ anomaly without conflicting the theoretical and experimental bounds.

Note that we have only considered the perturbativity limit on the massive spin-2 particle model in Ref. [27]. However, another criterion to determine if the perturbative calculation remains under control is the perturbative unitarity bound, which has a long history to restrict parameters in a given model [47,48]. Perhaps the most famous application was to limit the mass of the SM Higgs boson in Refs. [49–51]. An incomplete list of the use of unitarity bounds to restrict the BSM models includes Refs. [39,52–62].

In the present work, we would like to derive the unitarity bounds for the spin-2 particle model in Ref. [27]. Note that the interpretation of the muon $g-2$ anomaly involves G

[a] e-mail: dahuang@bao.ac.cn (corresponding author)
[b] e-mail: cqgeng@ucas.ac.cn
[c] e-mail: wujiajun@itp.ac.cn

Published online: 08 March 2024

couplings to charged leptons ℓ and photons γ. Thus, in order to constrain these two kinds of interactions, one needs to consider the 2-to-2 elastic scatterings of charged leptons and of photons via the mediation of G, with all possible initial and final helicity states. By yielding the s-wave projected amplitudes for all scattering processes, we can impose the unitarity bounds on the model parameters. As a result, it will be shown that the obtained unitarity bounds have significant impacts on the parameter space to explain the muon $g-2$.

The paper is organized as follows. In Sect. 2, we briefly summarize the main results in Ref. [27], including the Lagrangian of the spin-2 particle model and the leading-order expression of the muon $g-2$ contribution induced by G. Section 3 is devoted to the calculation of amplitudes for elastic scattering processes, $\ell^-\ell^+ \to \ell^-\ell^+$ and $\gamma\gamma \to \gamma\gamma$, with all possible initial and final helicity states. From these amplitudes, we derive the unitarity bounds on the charged-lepton- and photon-G couplings. We then make advantage of the obtained unitarity bounds to constrain the muon $g-2$ preferred parameter space in Sect. 4. Finally, we conclude and comment on the collider constraints in Sect. 5.

2 A spin-2 particle model and its explanation to lepton $g-2$

The Lagrangian for the spin-2 particle G explanation to the lepton $g-2$ is given by [63]

$$\mathcal{L}_G = -\frac{1}{\Lambda} G_{\mu\nu}\left[c_\gamma T_\gamma^{\mu\nu} + \sum_{\ell=e,\mu,\tau} c_\ell T_\ell^{\mu\nu}\right], \tag{2}$$

where the stress–energy tensors, $T_\ell^{\mu\nu}$ and $T_\gamma^{\mu\nu}$, of charged leptons and photons are defined by

$$\begin{aligned} T_\ell^{\mu\nu} &= \frac{i}{4}\bar{\ell}(\gamma^\mu\partial^\nu + \gamma^\nu\partial^\mu)\ell - \frac{i}{4}(\partial^\mu\bar{\ell}\gamma^\nu + \partial^\nu\bar{\ell}\gamma^\mu)\ell \\ &\quad -i\eta^{\mu\nu}\left[\bar{\ell}\gamma^\rho\partial_\rho\ell + im_\ell\bar{\ell}\ell - \frac{1}{2}\partial^\rho(\bar{\ell}\gamma_\rho\ell)\right], \\ T_\gamma^{\mu\nu} &= \frac{1}{4}\eta^{\mu\nu}F^{\rho\sigma}F_{\rho\sigma} - F^{\mu\rho}F_\rho^\nu \\ &\quad -\frac{1}{\xi}\left[\eta^{\mu\nu}\left(\partial^\rho\partial^\sigma A_\sigma A_\rho + \frac{1}{2}(\partial^\rho A_\rho)^2\right)\right. \\ &\quad \left. -\left(\partial^\mu\partial^\rho A_\rho A^\nu + \partial^\nu\partial^\rho A_\rho A^\mu\right)\right], \end{aligned} \tag{3}$$

respectively, with ξ the gauge parameter for the photon field. This Lagrangian can be viewed as a part of the low-energy effective action in the generalized Randall–Sundrum model where the massive spin-2 particle is the first KK excitation of the conventional graviton [28–32,39].

In the light of the effective interactions between G and charged leptons/photons in Eq. (2), we have drawn and calculated in Ref. [27] the one-loop Feynman diagrams contributing to the muon $g-2$, with the dominant contribution given by

$$\Delta a_\mu^G = \left(\frac{m_\mu^2}{\Lambda}\right)^2\left(\frac{\Lambda}{m_G}\right)^4\left(\frac{c_\mu^2}{48\pi^2} - \frac{c_\mu c_\gamma}{24\pi^2}\right). \tag{4}$$

When deriving this leading-order result, we have applied the loop regularization [45,46] method to regularize the quartic divergences of loop integrals, which has been shown to maintain the gauge invariance of quantum electrodynamics and the correct divergence structure simultaneously. Note that Graesser also calculated exactly the same Feynman diagrams in Ref. [64], and claimed that the loop integral for each Feynman diagram was logarithmically divergent. In the case with a universal coupling, even the logarithmically divergence was found to be cancelled out identically. It was argued in [64] that such a cancellation or the reduction of loop integral divergences was caused by the gravitational Ward identities. However, from our point of view, such the cancellation is accidental. Indeed, the Ward identities which are derived from the diffeomorphism invariance inherent to the massless graviton cannot be directly applied to the massive spin-2 particle. Technically, the calculation in Ref. [64] was performed with the dimensional regularization, which has been well known to be unable to respect the divergence structure of loop integrals, i.e., it would distort a power-law divergence into a logarithmic one. Thus, it is not appropriate to apply the dimensional regularization to the present situation with such high power-law divergent integrals.

Moreover, by requiring the validity of the perturbative expansion, i.e., the one-loop contributions to the lepton $g-2$ should dominate over the two-loop ones, we obtain novel constraints from the perturbativity on our non-renormalizable spin-2 particle interactions as follows

$$|c_\ell| < 4\pi\left(\frac{m_G}{\Lambda}\right)^2, \quad |c_\gamma| < 4\pi\left(\frac{m_G}{\Lambda}\right)^2, \tag{5}$$

which are obviously natural but non-trivial generalizations of perturbativity constraints on renormalizable operators [65].

3 Unitarity bounds

In this section, we apply the tree-level unitarity bounds as our criterion to determine whether our perturbative calculations remain under control, which can give extra constraints to our spin-2 particle model. Concretely, the unitarity of the S-matrix imposes the following bound to the s-wave projected amplitude $a_0(\sqrt{s})$ [50,59,62]

$$\mathrm{Re}(a_0)(\sqrt{s}) \le \frac{1}{2}, \tag{6}$$

where $a_0(\sqrt{s})$ is defined as

$$a_0(\sqrt{s}) = \sqrt{\frac{4|\mathbf{p}_i||\mathbf{p}_f|}{2^{\delta_i+\delta_f}s}}\frac{1}{32\pi}\int_{-1}^{1} d(\cos\theta)\mathcal{M}(i\to f) = \sqrt{\frac{4|\mathbf{p}_i||\mathbf{p}_f|}{2^{\delta_i+\delta_f}s}}\frac{1}{16\pi}\int_{-s}^{0}\frac{dt}{s}\mathcal{M}(i\to f), \tag{7}$$

in which the indices $\delta_{i,f} = 1$ if the two particles in the initial or final states are identical to each other, otherwise $\delta_{i,f} = 0$. In our model, we have two kinds of effective vertices: the photon and lepton couplings to the spin-2 particle G, so we need to compute the amplitudes for $\ell^-\ell^+ \to \ell^-\ell^+$ and $\gamma\gamma \to \gamma\gamma$ of various helicity assignments to determine their respective bounds.

3.1 $\ell^-\ell^+ \to \ell^-\ell^+$

We begin by considering the perturbative unitarity bounds for the lepton-G couplings c_ℓ with $\ell = e$, μ and τ, which can be derived from the amplitudes of $\ell^-\ell^+ \to \ell^-\ell^+$ of different $\ell^\pm$ helicity configurations. Given the Lagrangian in Eq. (2), there are two Feynman diagrams contributing to this process, which are shown in Fig. 1 with left and right panels corresponding to the s- and t-channels, respectively. Note that the lepton-G interaction in Eq. (2) is P-invariant, i.e., if the two scatterings of different helicity configurations are related by the parity P transformation, then they would be equal in amplitude. For example, we have the following relations

$$\mathcal{M}(\ell_R^-\ell_L^+ \to \ell_R^-\ell_L^+) = \mathcal{M}(\ell_L^-\ell_R^+ \to \ell_L^-\ell_R^+),$$
$$\mathcal{M}(\ell_R^-\ell_R^+ \to \ell_R^-\ell_R^+) = \mathcal{M}(\ell_L^-\ell_L^+ \to \ell_L^-\ell_L^+). \tag{8}$$

Also, we will work in the high-energy limit in which the lepton masses can be ignored compared with the external particle momenta. In what follows of this subsection, we shall present the detailed calculations of independent non-zero $\ell^-\ell^+ \to \ell^-\ell^+$ helicity amplitudes. By applying the unitarity bound on these amplitudes, we can obtain constraints on c_ℓ.

3.1.1 $\ell_R^-\ell_L^+ \to \ell_R^-\ell_L^+$

Let us begin by computing the amplitude of $\ell_R^-\ell_L^+ \to \ell_R^-\ell_L^+$. In the massless limit, the momenta of external particles in the center-of-mass (com) frame are given by:

$$\begin{aligned}
&\text{Incoming}: \quad \ell_R^-: \quad p_1 = (E,0,0,E),\\
&\qquad\qquad\ \ \ell_L^+: \quad p_2 = (E,0,0,-E)\\
&\text{Outgoing}: \quad \ell_R^-: \quad k_1 = (E,E\sin\theta,0,E\cos\theta),\\
&\qquad\qquad\ \ \ell_L^+: \quad k_2 = (E,-E\sin\theta,0,-E\cos\theta),
\end{aligned} \tag{9}$$

while the polarization vectors are denoted as

$$\begin{aligned}
\text{Incoming}: u_R(p_1) &= \sqrt{2E}\begin{pmatrix}0\\0\\1\\0\end{pmatrix},\\
v_L(p_2) &= \sqrt{2E}\begin{pmatrix}0\\0\\0\\-1\end{pmatrix},\\
\text{Outgoing}: u_R(k_1) &= \sqrt{2E}\begin{pmatrix}0\\0\\\cos\frac{\theta}{2}\\\sin\frac{\theta}{2}\end{pmatrix},\\
v_L(k_2) &= \sqrt{2E}\begin{pmatrix}0\\0\\\sin\frac{\theta}{2}\\-\cos\frac{\theta}{2}\end{pmatrix}.
\end{aligned} \tag{10}$$

The total amplitude is composed of the s- and t-channel ones. The s-channel amplitude is given by

$$\begin{aligned}
&i\mathcal{M}_s(\ell_R^-\ell_L^+ \to \ell_R^-\ell_L^+)\\
&= -\frac{ic_\ell^2}{32\Lambda^2}\bar{v}_L(p_2)[\gamma^\mu(p_1^\nu - p_2^\nu) + \gamma^\nu(p_1^\mu - p_2^\mu)\\
&\quad -2\eta^{\mu\nu}(\not{p}_1 - \not{p}_2 - 2m_\ell)]u_R(p_1)\\
&\quad \times\bar{u}_R(k_1)[\gamma^\rho(k_1^\sigma - k_2^\sigma) + \gamma^\sigma(k_1^\rho - k_2^\rho)\\
&\quad -2\eta^{\rho\sigma}(\not{k}_1 - \not{k}_2 - 2m_\ell)]v_L(k_2)\frac{B_{\mu\nu,\rho\sigma}}{Q^2 - m_G^2}.
\end{aligned} \tag{11}$$

By using the external particles' equations of motion $\not{p}_1 u_R(p_1) = m_\ell u_R(p_1) \simeq 0$ and $\not{p}_2 v_L(p_2) = -m_\ell v_L(p_2) \simeq 0$ where the symbol $\simeq$ represents the massless limit, the above s-channel amplitude can be simplified to

$$\begin{aligned}
&i\mathcal{M}_s(\ell_R^-\ell_L^+ \to \ell_R^-\ell_L^+)\\
&= -\frac{ic_\ell^2}{8\Lambda^2}\big\{(p_1 - p_2)(k_1 - k_2)[\bar{u}_R(k_1)\gamma^\mu v_L(k_2)]\\
&\quad \times[\bar{v}_L(p_2)\gamma_\mu u_R(p_1)]\\
&\quad +[\bar{u}_R(k_1)(\not{p}_1 - \not{p}_2)v_L(k_2)][\bar{v}_L(p_2)(\not{k}_1 - \not{k}_2)u_R(p_1)]\big\}\\
&\quad \times\frac{1}{Q^2 - m_G^2}.
\end{aligned} \tag{12}$$

Now we turn to compute the fermion current in this s-channel $\ell_R^-\ell_L^+ \to \ell_R^-\ell_L^+$ process. Note that

$$\gamma^0\gamma^\mu = \begin{pmatrix}0&1\\1&0\end{pmatrix}\begin{pmatrix}0&\sigma^\mu\\\bar{\sigma}^\mu&0\end{pmatrix} = \begin{pmatrix}\bar{\sigma}^\mu&0\\0&\sigma^\mu\end{pmatrix}. \tag{13}$$

Thus, for a vector-like current there are only two kinds of nonzero chirality configurations for (ℓ^-, ℓ^+) pairs: (L, R) and (R, L), while other two configurations like (L, L) and

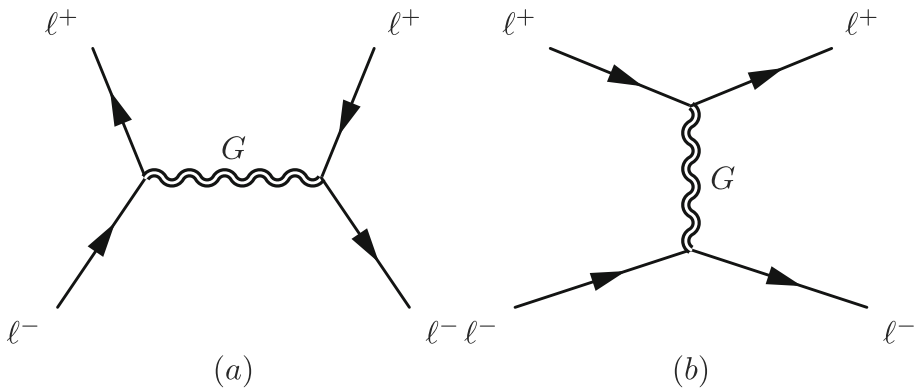

Fig. 1 Feynman diagrams which give rise to the scattering process $\ell^-\ell^+ \to \ell^-\ell^+$

(R, R) are zero. Hence, for a $\ell_R^-\ell_L^+$ pair, the corresponding current given by

$$\begin{aligned}\bar{v}_L(p_2)\gamma^\mu u_R(p_1) &= (2E)(0,-1)\sigma^\mu \begin{pmatrix}1\\0\end{pmatrix}\\ &= (2E)(0,-1,-i,0),\\ \bar{v}_L(k_2)\gamma^\mu u_R(k_1) &= (2E)\left(\sin\frac{\theta}{2}, -\cos\frac{\theta}{2}\right)\sigma^\mu \begin{pmatrix}\cos\frac{\theta}{2}\\ \sin\frac{\theta}{2}\end{pmatrix}\\ &= (2E)(0,-\cos\theta,-i,\sin\theta), \end{aligned} \tag{14}$$

so that

$$\begin{aligned}&[\bar{u}_R(k_1)\gamma^\mu v_L(k_2)][\bar{v}_L(p_2)\gamma_\mu u_R(p_1)]\\ &\quad = -(2E)^2(1+\cos\theta) = 2u, \end{aligned} \tag{15}$$

$$\bar{v}_L(p_2)(\not{k}_1 - \not{k}_2)u_R(p_1) = (2E)^2\sin\theta = s\sin\theta, \tag{16}$$

$$\bar{u}_R(k_1)(\not{p}_1 - \not{p}_2)v_L(k_2) = -(2E)^2\sin\theta = -s\sin\theta. \tag{16}$$

Consequently, the s-channel amplitude can be given by

$$\begin{aligned} i\mathcal{M}_s &= -\frac{4ic_\ell^2}{32\Lambda^2}\frac{\left(2u(u-t) - s^2\sin^2\theta\right)}{s-m_G^2}\\ &= -\frac{ic_\ell^2}{4\Lambda^2}\frac{u(u-3t)}{s-m_G^2} = -\frac{ic_\ell^2}{4\Lambda^2}\frac{(s+t)(s+4t)}{s-m_G^2}, \end{aligned} \tag{17}$$

where in the last equality we have used the following relations

$$\begin{aligned} s(1+\cos\theta) = -2u, \quad s(1-\cos\theta) = -2t,\\ 4ut = s^2\sin^2\theta. \end{aligned} \tag{18}$$

Now we come to compute t-channel contribution, with the amplitude given by

$$\begin{aligned} &i\mathcal{M}_t(\ell_R^-\ell_L^+ \to \ell_R^-\ell_L^+)\\ &= -\frac{ic_\ell^2}{32\Lambda^2}\bar{v}_L(p_2)[\gamma^\mu(-p_2^\nu - k_2^\nu) + \gamma^\nu(-p_2^\mu - k_2^\mu)\\ &\quad -2\eta^{\mu\nu}(-\not{p}_2 - \not{k}_2 - 2m_\ell)]v_L(k_2)\\ &\quad \times\bar{u}_R(k_1)[\gamma^\rho(p_1^\sigma + k_1^\sigma) + \gamma^\sigma(p_1^\rho + k_1^\rho)\\ &\quad -2\eta^{\rho\sigma}(\not{p}_1 + \not{k}_1 - 2m_\ell)]u_R(p_1)\frac{B_{\mu\nu,\rho\sigma}}{q^2 - m_G^2}. \end{aligned} \tag{19}$$

By using the lepton on-shell conditions, the t-channel amplitude can be reduced into

$$\begin{aligned} &i\mathcal{M}_t(\ell_R^-\ell_L^+ \to \ell_R^-\ell_L^+)\\ &= \frac{4ic_\ell^2}{32\Lambda^2}\frac{1}{q^2-m_G^2}\big\{(k_1+p_1)(k_2+p_2)\\ &\quad \times[\bar{u}_R(k_1)\gamma^\mu u_R(p_1)][\bar{v}_L(p_2)\gamma_\mu v_L(k_2)]\\ &\quad +[\bar{u}_R(k_1)(\not{k}_2 + \not{p}_2)u_R(p_1)]\\ &\quad \times[\bar{v}_L(p_2)(\not{k}_1 + \not{p}_1)v_L(k_2)]\big\}. \end{aligned} \tag{20}$$

In the center of mass frame, the t-channel amplitude can be further simplified to

$$\begin{aligned} i\mathcal{M}_t(\ell_R^-\ell_L^+ \to \ell_R^-\ell_L^+) &= \frac{ic_\ell^2}{4\Lambda^2}\frac{u(u-3s)}{t-m_G^2}\\ &= \frac{ic_\ell^2}{4\Lambda^2}\frac{(t+s)(t+4s)}{t-m_G^2}. \end{aligned} \tag{21}$$

Therefore, the total amplitude is given by summing over the s- and t-channel amplitudes:

$$\begin{aligned} &i\mathcal{M}(\ell_R^-\ell_L^+ \to \ell_R^-\ell_L^+)\\ &= -\frac{ic_\ell^2}{4\Lambda^2}\left[\frac{u(u-3t)}{s-m_G^2} - \frac{u(u-3s)}{t-m_G^2}\right]\\ &= -\frac{ic_\ell^2}{4\Lambda^2}\left[\frac{(s+t)(s+4t)}{s-m_G^2} - \frac{(t+s)(t+4s)}{t-m_G^2}\right]. \end{aligned} \tag{22}$$

Here the minus sign between the two terms in the bracket can be understood to come from the interchange the two external fermion particles of momenta k_1 and p_2.

3.1.2 $\ell_R^-\ell_L^+ \to \ell_L^-\ell_R^+$

Now we consider another kinematic configuration $\ell_R^-\ell_L^+ \to \ell_L^-\ell_R^+$, in which the four momenta are denoted by

$$\begin{aligned} p_1^\mu &= (E,0,0,E), \quad p_2^\nu = (E,0,0,-E),\\ k_1^\rho &= (E, E\sin\theta, 0, E\cos\theta),\\ k_2^\sigma &= (E, -E\sin\theta, 0, -E\cos\theta), \end{aligned} \tag{23}$$

while their polarization spinors are given by

$$u_L(k_1)=\sqrt{2E}\begin{pmatrix}\xi_L\\0\end{pmatrix}=\sqrt{2E}\begin{pmatrix}-\sin\frac{\theta}{2}\\\cos\frac{\theta}{2}\\0\\0\end{pmatrix},$$
$$v_R(k_2)=\sqrt{2E}\begin{pmatrix}\eta_L\\0\end{pmatrix}=\sqrt{2E}\begin{pmatrix}\cos\frac{\theta}{2}\\\sin\frac{\theta}{2}\\0\\0\end{pmatrix}. \tag{24}$$

For the s-channel, the amplitude after taking into account the on-shell condition can also be reduced to Eq. (12), so that by using the explicit expressions for momenta and polarization spinors of external particles, we have

$$\begin{aligned}\bar{v}_L(p_2)\gamma^\mu u_R(p_1)&=(2E)(0,-1)\sigma^\mu\begin{pmatrix}1\\0\end{pmatrix}\\&=(2E)(0,-1,-i,0),\\\bar{u}_L(k_1)\gamma^\mu v_R(k_2)&=(2E)\left(-\sin\frac{\theta}{2},\cos\frac{\theta}{2}\right)\bar{\sigma}^\mu\begin{pmatrix}\cos\frac{\theta}{2}\\\sin\frac{\theta}{2}\end{pmatrix}\\&=(0,-\cos\theta,-i,\sin\theta),\end{aligned} \tag{25}$$

and

$$\begin{aligned}\left[\bar{u}_L(k_1)\gamma^\mu v_R(k_2)\right]\left[\bar{v}_L(p_2)\gamma_\mu u_R(p_1)\right]&=(2E)^2(1-\cos\theta)\\&=-2t,\\\bar{u}_L(k_1)(\not{p}_1-\not{p}_2)v_R(k_2)&=-(2E)^2\sin\theta,\\\bar{v}_L(p_2)(\not{k}_1-\not{k}_2)u_R(p_1)&=(2E)^2\sin\theta.\end{aligned} \tag{26}$$

Therefore, the s-channel amplitude is given by

$$i\mathcal{M}_s(\ell_R^-\ell_L^+\to\ell_L^-\ell_R^+)=-\frac{ic_\ell^2}{4\Lambda^2}\frac{t(t-3u)}{s-m_G^2}. \tag{27}$$

Note that the bi-spinor forms like $\bar{u}_L(k_1)\gamma^\mu u_R(p_1)=0$ or $\bar{v}_L(p_2)\gamma^\mu v_R(k_2)=0$ vanish, so that we cannot write down the t-channel amplitude. Thus, the total amplitude of $\ell_R^-\ell_L^+\to\ell_L^-\ell_R^+$ is given by its s-channel one, with the following final result

$$\begin{aligned}i\mathcal{M}(\ell_R^-\ell_L^+\to\ell_L^-\ell_R^+)&=i\mathcal{M}_s(\ell_R^-\ell_L^+\to\ell_L^-\ell_R^+)\\&=-\frac{ic_\ell^2}{4\Lambda^2}\frac{t(t-3u)}{s-m_G^2}.\end{aligned} \tag{28}$$

3.1.3 $\ell_R^-\ell_R^+\to\ell_R^-\ell_R^+$

Since we cannot write the bi-spinors, such as $\bar{v}_R(p_2)\gamma^\mu u_R(p_1)$ or $\bar{u}_R(k_1)\gamma^\mu v_R(k_2)$, the s-channel diagram cannot provide any contribution to this kinematic configuration. However, the t-channel Feynman diagram does contribute, and in the following we would like to compute it. By using the on-shell conditions, we can simplify the t-channel amplitude into the following form

$$\begin{aligned}i\mathcal{M}_t(\ell_R^-\ell_R^+\to\ell_R^-\ell_R^+)&=\frac{ic_\ell^2}{8\Lambda^2}\frac{1}{q^2-m_G^2}\\&\times\Big\{(k_1+p_1)(k_2+p_2)[\bar{u}_R(k_1)\gamma^\mu u_R(k_2)]\\&\times[\bar{v}_R(p_2)\gamma_\mu v_R(k_2)]\\&+[\bar{u}_R(k_1)(\not{p}_2+\not{k}_2)u_R(p_1)][\bar{v}_R(p_2)(\not{p}_1+\not{k}_1)v_R(k_2)]\Big\}.\end{aligned} \tag{29}$$

Here by taking the explicit form of momenta and spinors in the com frame, we can obtain

$$\begin{aligned}&\bar{u}_R(k_1)\gamma^\mu u_R(p_1)\\&=(2E)\left(\cos\frac{\theta}{2},\sin\frac{\theta}{2}\right)\sigma^\mu\begin{pmatrix}1\\0\end{pmatrix}\\&=(2E)\left(\cos\frac{\theta}{2},\sin\frac{\theta}{2},i\sin\frac{\theta}{2},\cos\frac{\theta}{2}\right),\\&\bar{v}_R(p_2)\gamma^\mu v_R(k_2)=(2E)(1,0)\bar{\sigma}^\mu\begin{pmatrix}\cos\frac{\theta}{2}\\\sin\frac{\theta}{2}\end{pmatrix}\\&=(2E)\left(\cos\frac{\theta}{2},-\sin\frac{\theta}{2},i\sin\frac{\theta}{2},-\cos\frac{\theta}{2}\right),\end{aligned} \tag{30}$$

so that

$$\begin{aligned}[\bar{u}_R(k_1)\gamma^\mu u_R(p_1)][\bar{v}_R(p_2)\gamma_\mu v_R(k_2)]&=2(2E)^2=2s,\\\bar{u}_R(k_1)(\not{p}_2+\not{k}_2)u_R(p_1)&=2(2E)^2\cos\frac{\theta}{2},\\\bar{v}_R(p_2)(\not{p}_1+\not{k}_1)v_R(k_2)&=2(2E)^2\cos\frac{\theta}{2}.\end{aligned} \tag{31}$$

It turns out that the final expression for the amplitude of $\ell_R^-\ell_R^+\to\ell_R^-\ell_R^+$ is given by

$$\begin{aligned}i\mathcal{M}(\ell_R^-\ell_R^+\to\ell_R^-\ell_R^+)&=i\mathcal{M}_t(\ell_R^-\ell_R^+\to\ell_R^-\ell_R^+)\\&=\frac{ic_\ell^2}{4\Lambda^2}\frac{s(s-3u)}{t-m_G^2}.\end{aligned} \tag{32}$$

3.1.4 Unitarity bounds for $\ell^-\ell^+\to\ell^-\ell^+$

In the above discussion, we obtains all of the nonzero $\ell^-\ell^+\to\ell^-\ell^+$ amplitudes of different helicity configurations, which are summarized again as follows

$$\begin{aligned}\mathcal{M}(\ell_R^-\ell_L^+\to\ell_R^-\ell_L^+)&=\mathcal{M}(\ell_L^-\ell_R^+\to\ell_L^-\ell_R^+)\\&=-\frac{c_\ell^2}{4\Lambda^2}\left[\frac{u(u-3t)}{s-m_G^2}-\frac{u(u-3s)}{t-m_G^2}\right],\\\mathcal{M}(\ell_R^-\ell_R^+\to\ell_R^-\ell_R^+)&=\mathcal{M}(\ell_L^-\ell_L^+\to\ell_L^-\ell_L^+)\\&=\frac{c_\ell^2}{4\Lambda^2}\frac{s(s-3u)}{t-m_G^2},\end{aligned}$$

$$\mathcal{M}(\ell_R^-\ell_L^+ \to \ell_L^-\ell_R^+) = \mathcal{M}(\ell_L^-\ell_R^+ \to \ell_R^-\ell_L^+) = -\frac{c_\ell^2}{4\Lambda^2}\frac{t(t-3u)}{s-m_G^2}, \tag{33}$$

where the two amplitudes in a single line are P-symmetric to one another, while other helicity configurations would lead to vanishing amplitudes. By using the definition of $a_0(\sqrt{s})$ in Eq. (7), we can obtain the s-wave projected amplitudes, given by

$$\begin{aligned}
a_0(\ell_R^-\ell_L^+ \to \ell_R^-\ell_L^+) &= a_0(\ell_L^-\ell_R^+ \to \ell_L^-\ell_R^+) \\
&= -\frac{1}{16\pi s}\frac{c_\ell^2}{4\Lambda^2}\left[-\frac{s(28s^2-21m_G^2 s-6m_G^4)}{6(s-m_G^2)}\right. \\
&\quad \left.+(4s+m_G^2)(s+m_G^2)\ln\left(\frac{s+m_G^2}{m_G^2}\right)\right] \\
&\approx \frac{c_\ell^2}{16\pi}\frac{s}{4\Lambda^2}\left(\frac{14}{3}-4\ln\frac{s}{m_G^2}\right) \sim \frac{c_\ell^2}{16\pi}\left(\frac{14}{3}-4\ln\frac{4\Lambda^2}{m_G^2}\right), \\
a_0(\ell_R^-\ell_R^+ \to \ell_R^-\ell_R^+) &= a_0(\ell_L^-\ell_L^+ \to \ell_L^-\ell_L^+) \\
&= \frac{1}{16\pi}\frac{c_\ell^2}{4\Lambda^2}\left[3s-(4s+3m_G^2)\ln\left(\frac{s+m_G^2}{m_G^2}\right)\right] \\
&\approx \frac{c_\ell^2}{16\pi}\frac{s}{4\Lambda^2}\left(3-4\ln\frac{s}{m_G^2}\right) \\
&\sim \frac{c_\ell^2}{16\pi}\left(3-4\ln\frac{4\Lambda^2}{m_G^2}\right), \\
a_0(\ell_R^-\ell_L^+ \to \ell_L^-\ell_R^+) &= a_0(\ell_L^-\ell_R^+ \to \ell_R^-\ell_L^+) \\
&= \frac{1}{16\pi}\frac{c_\ell^2}{4\Lambda^2}\frac{s^2}{6(s-m_G^2)} \approx \frac{1}{16\pi}\frac{c_\ell^2}{6}\frac{s}{4\Lambda^2} \sim \frac{c_\ell^2}{96\pi},
\end{aligned} \tag{34}$$

where the symbol $\sim$ denotes the high energy limit with $s \to 4\Lambda^2$. By requiring the s-wave projected amplitudes to satisfy the unitarity bound $\mathrm{Re}[a_0(\sqrt{s})] \le 1/2$, we can obtain the following constraints on the Wilsonian coefficient c_ℓ

$$\ell_R^-\ell_L^+ \to \ell_R^-\ell_L^+ : \quad c_\ell \le \sqrt{\frac{8\pi}{\left|\frac{14}{3}-4\ln\frac{4\Lambda^2}{m_G^2}\right|}}, \tag{35}$$

$$\ell_R^-\ell_L^+ \to \ell_L^-\ell_R^+ : \quad c_\ell \le \sqrt{48\pi}, \tag{36}$$

$$\ell_R^-\ell_R^+ \to \ell_R^-\ell_R^+ : \quad c_\ell \le \sqrt{\frac{8\pi}{\left|3-4\ln\frac{4\Lambda^2}{m_G^2}\right|}}. \tag{37}$$

In Fig. 2, we plot the upper limits on c_ℓ derived from different helicity states, which are functions of the spin-2 particle mass m_G when $\Lambda = 1$ TeV. It is seen that the most stringent constraint on c_ℓ is given by the channel $\ell_R^-\ell_R^+ \to \ell_R^-\ell_R^+$ ($\ell_L^-\ell_L^+ \to \ell_L^-\ell_L^+$) in the spin-2 particle mass range from 100 GeV to 500 GeV, which is of great interest to in the interpretation of the muon $g-2$ anomaly.

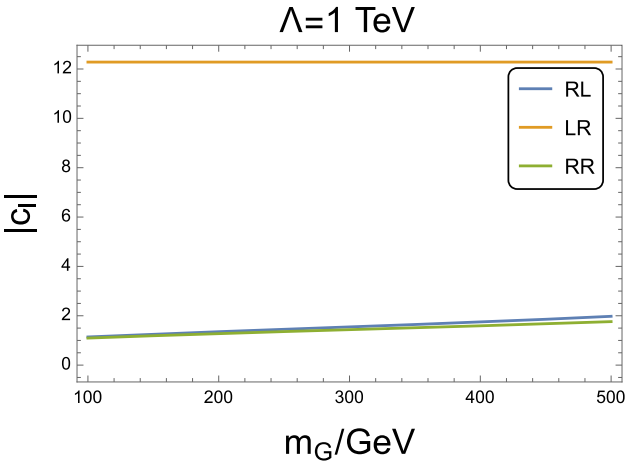

Fig. 2 The unitarity bounds on the lepton-G Wilsonian coefficients c_ℓ for the three independent helicity configurations: $\ell_R^-\ell_L^+ \to \ell_R^-\ell_L^+$, $\ell_R^-\ell_L^+ \to \ell_L^-\ell_R^+$ and $\ell_R^-\ell_R^+ \to \ell_R^-\ell_R^+$, which are labeled as RL, LR, and RR in the legend

3.2 $\gamma\gamma \to \gamma\gamma$

In order to obtain the unitarity bounds on the photon-G coupling c_γ, we have to calculate the $\gamma\gamma \to \gamma\gamma$ amplitudes of various polarization configurations. The relevant Feynman diagrams are shown in Fig. 3, which correspond to the s-, t-, and u-channels, respectively. As the photon-G vertex in Eq. (2) preserves the spatial parity P symmetry, the amplitudes of different photon polarizations are the same to each other when they are related by parity transformation, which greatly reduces the number of independent photon 2-to-2 scattering amplitudes. In this subsection, we compute these independent nonzero photon scattering amplitudes, based on which we can yield the associated unitarity bounds on c_γ.

3.2.1 $\gamma_R\gamma_R \to \gamma_R\gamma_R$

Firstly, we consider the amplitude of $\gamma_R\gamma_R \to \gamma_R\gamma_R$, where the four external photons are all right-handed. In the com frame, the two incoming photons are specified by

$$\begin{aligned}
p_1^\mu &= (E,0,0,E), \quad \epsilon_R^\mu(p_1) = \frac{1}{\sqrt{2}}(0,-1,-i,0), \\
p_2^\nu &= (E,0,0,-E), \quad \epsilon_R^\nu(p_2) = \frac{1}{\sqrt{2}}(0,1,-i,0),
\end{aligned} \tag{38}$$

while the two outgoing photons are represented by

$$\begin{aligned}
k_1^\rho &= (E, E\sin\theta, 0, E\cos\theta), \\
\epsilon_R^*(k_1) &= \frac{1}{\sqrt{2}}(0,-\cos\theta, i, \sin\theta), \\
k_2^\sigma &= (E, -E\sin\theta, 0, -E\cos\theta), \\
\epsilon_R^*(k_2) &= \frac{1}{\sqrt{2}}(0,\cos\theta, i, -\sin\theta).
\end{aligned} \tag{39}$$

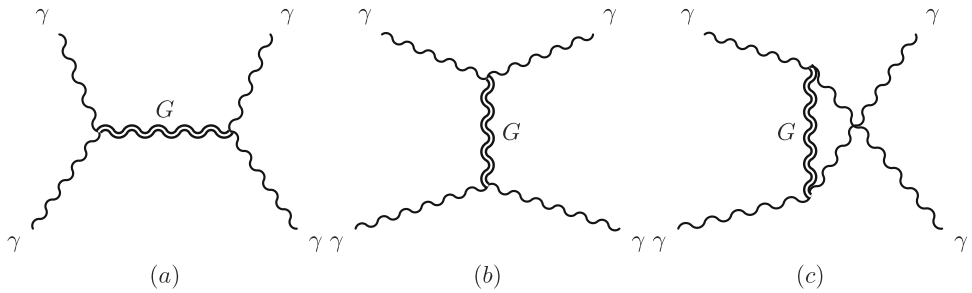

Fig. 3 Feynman diagrams for the photon–photon scattering process of $\gamma\gamma \to \gamma\gamma$

The amplitude constitutes three Feynman diagrams shown in Fig. 3, corresponding to s-, t- and u-channels, respectively. In the following, we shall calculate them one by one. According to the Feynman rules, the s-channel amplitude is given by

$$\begin{aligned} &i\mathcal{M}_s(\gamma_R\gamma_R \to \gamma_R\gamma_R) \\ &= -\frac{ic_\gamma^2}{2\Lambda^2}\epsilon_R^\mu(p_1)\epsilon_R^\nu(p_2)\epsilon_R^*(k_1)\epsilon_R^*(k_2)[(p_1\cdot p_2)C_{\alpha\beta,\mu\nu} \\ &\quad + D_{\alpha\beta,\mu\nu}(p_1,p_2)] \\ &\quad \times \frac{B^{\alpha\beta,\lambda\delta}(Q)}{Q^2-m_G^2}[(k_1\cdot k_2)C_{\lambda\delta,\rho\sigma} + D_{\lambda\delta,\rho\sigma}(k_1,k_2)]. \end{aligned} \tag{40}$$

Note that, by using the relation $Q = p_1 + p_2 = k_1 + k_2$, we find that terms proportional to four- and two-powers of $1/m_G$ are canceled. By further making use of the specific momenta and polarization vectors of the four external particles in Eqs. (38) and (39), the s-channel amplitude vanishes, while the t- and u-channel amplitudes are given by

$$\begin{aligned} &i\mathcal{M}_t(\gamma_R\gamma_R \to \gamma_R\gamma_R) \\ &= -\frac{ic_\gamma^2}{2\Lambda^2}\epsilon_R^\mu(p_1)\epsilon_R^\nu(p_2)\epsilon_R^*(k_1)\epsilon_R^*(k_2)[(-p_1\cdot k_1)C_{\alpha\beta,\mu\rho} \\ &\quad + D_{\alpha\beta,\mu\rho}(p_1,-k_1)] \\ &\quad \times \frac{B^{\alpha\beta,\lambda\delta}(q)}{q^2-m_G^2}[(-p_2\cdot k_2)C_{\lambda\delta,\nu\sigma} + D_{\lambda\delta,\nu\sigma}(p_2,-k_2)] \\ &= -\frac{ic_\gamma^2}{2\Lambda^2}\frac{2s^2}{t-m_G^2}, \end{aligned} \tag{41}$$

$$\begin{aligned} &i\mathcal{M}_u(\gamma_R\gamma_R \to \gamma_R\gamma_R) \\ &= -\frac{ic_\gamma^2}{2\Lambda^2}\epsilon_R^\mu(p_1)\epsilon_R^\nu(p_2)\epsilon_R^*(k_1)\epsilon_R^*(k_2)[(-p_1\cdot k_2)c_{\alpha\beta,\mu\rho} \\ &\quad + D_{\alpha\beta,\mu\rho}(p_1,-k_2)] \\ &\quad \times \frac{B^{\alpha\beta,\lambda\delta}(q')}{q'^2-m_G^2}[(-p_2\cdot k_1)C_{\lambda\delta,\nu\sigma} + D_{\lambda\delta,\nu\sigma}(p_2,-k_1)] \\ &= -\frac{ic_\gamma^2}{2\Lambda^2}\frac{2s^2}{u-m_G^2}, \end{aligned} \tag{42}$$

where $q \equiv p_1 - k_1 = k_2 - p_2$ and $q' = p_1 - k_2 = k_1 - p_2$, so that $q^2 = t$ and $q'^2 = u$. Therefore, the total amplitude of $\gamma_R\gamma_R \to \gamma_R\gamma_R$ is written as

$$i\mathcal{M}(\gamma_R\gamma_R \to \gamma_R\gamma_R) = -\frac{iC_\gamma^2}{2\Lambda^2}\left(\frac{2s^2}{t-m_G^2} + \frac{2s^2}{u-m_G^2}\right). \tag{43}$$

3.2.2 $\gamma_R\gamma_L \to \gamma_R\gamma_L$

We now turn to the process of $\gamma_R\gamma_L \to \gamma_R\gamma_L$. In the com frame, we can define the polarization vectors of the incoming particles as follows

$$\epsilon_R^\mu(p_1) = \frac{1}{\sqrt{2}}(0,-1,-i,0), \quad \epsilon_L^\nu = \frac{1}{\sqrt{2}}(0,-1,-i,0), \tag{44}$$

while those of the outgoing particles are given by

$$\begin{aligned} \epsilon_R^*(k_1) &= \frac{1}{\sqrt{2}}(0,-\cos\theta,i,\sin\theta), \\ \epsilon_L^*(k_2) &= \frac{1}{\sqrt{2}}(0,-\cos\theta,i,\sin\theta). \end{aligned} \tag{45}$$

By taking the above expressions of the polarization vectors and momenta of the external particles into formulas for the s-, t- and u-channels, we can easily obtain the following partial amplitudes

$$\begin{aligned} i\mathcal{M}_s(\gamma_R\gamma_L \to \gamma_R\gamma_L) &= -\frac{ic_\gamma^2}{2\Lambda^2}\frac{2u^2}{s-m_G^2}, \\ i\mathcal{M}_t(\gamma_R\gamma_L \to \gamma_R\gamma_L) &= -\frac{ic_\gamma^2}{2\Lambda^2}\frac{2u^2}{t-m_G^2}, \\ i\mathcal{M}_u(\gamma_R\gamma_L \to \gamma_R\gamma_L) &= 0. \end{aligned} \tag{46}$$

Thus, the total amplitude is the summation over the s-, t- and u-channels

$$i\mathcal{M}(\gamma_R\gamma_L \to \gamma_R\gamma_L) = -\frac{ic_\gamma^2}{2\Lambda^2}\left(\frac{2u^2}{s-m_G^2} + \frac{2u^2}{t-m_G^2}\right). \tag{47}$$

3.2.3 $\gamma_R\gamma_L \to \gamma_L\gamma_R$

In the case of $\gamma_R\gamma_L \to \gamma_L\gamma_R$, the polarization vectors for the external photons in the com frame are given by

$$\begin{aligned} \epsilon_R(p_1) &= \frac{1}{\sqrt{2}}(0,-1,-i,0), \\ \epsilon_L(p_2) &= \frac{1}{\sqrt{2}}(0,-1,-i,0), \\ \epsilon_L^*(k_1) &= \frac{1}{\sqrt{2}}(0,\cos\theta,i-\sin\theta), \end{aligned}$$

$$\epsilon_R^*(k_2) = \frac{1}{\sqrt{2}}(0, \cos\theta, i, -\sin\theta). \tag{48}$$

Following exactly the same procedure in the previous subsections, we can derive the following amplitudes for the s-, t- and u-channels of $\gamma_R\gamma_L \to \gamma_L\gamma_R$:

$$\begin{aligned} i\mathcal{M}_s(\gamma_R\gamma_L \to \gamma_L\gamma_R) &= -\frac{ic_\gamma^2}{2\Lambda^2}\frac{2t^2}{s-m_G^2}, \\ i\mathcal{M}_t(\gamma_R\gamma_L \to \gamma_L\gamma_R) &= 0, \\ i\mathcal{M}_u(\gamma_R\gamma_L \to \gamma_L\gamma_R) &= -\frac{ic_\gamma^2}{2\Lambda^2}\frac{2t^2}{u-m_G^2}. \end{aligned} \tag{49}$$

It turns out that the total amplitude of $\gamma_R\gamma_L \to \gamma_L\gamma_R$ is given by

$$i\mathcal{M}(\gamma_R\gamma_L \to \gamma_L\gamma_R) = -\frac{ic_\gamma^2}{2\Lambda^2}\left(\frac{2t^2}{s-m_G^2} + \frac{2t^2}{u-m_G^2}\right). \tag{50}$$

3.2.4 Unitarity bounds for $\gamma\gamma \to \gamma\gamma$

Here we summarize the nonzero independent $\gamma\gamma \to \gamma\gamma$ amplitudes of different polarizations as follows

$$\begin{aligned} i\mathcal{M}(\gamma_R\gamma_L \to \gamma_R\gamma_L) &= i\mathcal{M}(\gamma_L\gamma_R \to \gamma_L\gamma_R) \\ &= -\frac{ic_\gamma^2}{2\Lambda^2}\left(\frac{2u^2}{s-m_G^2} + \frac{2u^2}{t-m_G^2}\right), \\ i\mathcal{M}(\gamma_R\gamma_L \to \gamma_L\gamma_R) &= i\mathcal{M}(\gamma_L\gamma_R \to \gamma_R\gamma_L) \\ &= -\frac{ic_\gamma^2}{2\Lambda^2}\left(\frac{2t^2}{s-m_G^2} + \frac{2t^2}{u-m_G^2}\right), \\ i\mathcal{M}(\gamma_R\gamma_R \to \gamma_R\gamma_R) &= i\mathcal{M}(\gamma_L\gamma_L \to \gamma_L\gamma_L) \\ &= -\frac{ic_\gamma^2}{2\Lambda^2}\left(\frac{2s^2}{t-m_G^2} + \frac{2s^2}{u-m_G^2}\right), \end{aligned} \tag{51}$$

while all other polarization amplitudes vanish identically. According to the definition of $a_0(\sqrt{s})$ in Eq. (7), the s-wave projected amplitudes for the nontrivial polarization assignments are given by

$$\begin{aligned} &a_0(\gamma_R\gamma_R \to \gamma_R\gamma_R) = a_0(\gamma_L\gamma_L \to \gamma_L\gamma_L) \\ &= \frac{c_\gamma^2}{4\pi}\frac{s}{4\Lambda^2}\ln\frac{s+m_G^2}{m_G^2} \approx \frac{c_\gamma^2}{4\pi}\frac{s}{4\Lambda^2}\ln\frac{s}{m_G^2} \sim \frac{c_\gamma^2}{4\pi}\ln\frac{4\Lambda^2}{m_G^2}, \\ &a_0(\gamma_R\gamma_L \to \gamma_R\gamma_L) = a_0(\gamma_R\gamma_L \to \gamma_L\gamma_R) \\ &= a_0(\gamma_L\gamma_R \to \gamma_L\gamma_R) = a_0(\gamma_L\gamma_R \to \gamma_R\gamma_L) \\ &= -\frac{1}{32\pi s}\frac{c_\gamma^2}{\Lambda^2}\left[\frac{s(11s^2 - 3m_G^2 s - 6m_G^4)}{6(s-m_G^2)}\right. \\ &\quad \left. -(s+m_G^2)\ln\frac{s+m_G^2}{m_G^2}\right] \end{aligned}$$

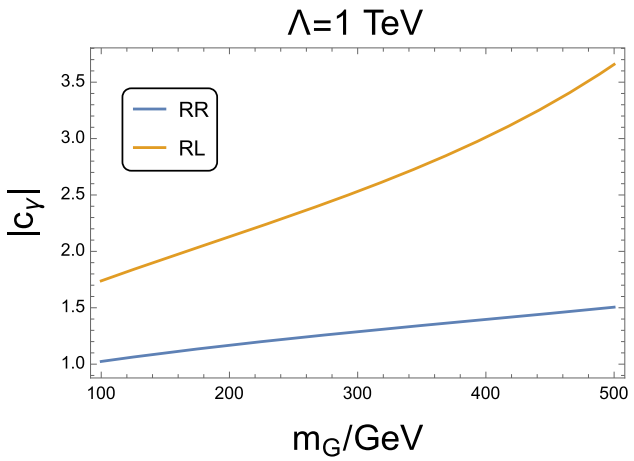

Fig. 4 The unitarity bounds on the photon-G Wilsonian coefficient c_γ for two independent helicity configurations: $\gamma_R\gamma_R \to \gamma_R\gamma_R$ and $\gamma_R\gamma_L \to \gamma_R\gamma_L$, which are labeled as RR and RL in the legend

$$\approx -\frac{c_\gamma^2}{8\pi}\frac{s}{4\Lambda^2}\left(\frac{11}{6} - \ln\frac{s}{m_G^2}\right) \sim -\frac{c_\gamma^2}{8\pi}\left(\frac{11}{6} - \ln\frac{4\Lambda^2}{m_G^2}\right), \tag{52}$$

where we have taken the high-energy limit with $s \sim 4\Lambda^2 \gg m_G^2$. Therefore, the unitarity bounds for these channels are given by

$$\gamma_R\gamma_R \to \gamma_R\gamma_R: \quad c_\gamma \lesssim \sqrt{\frac{2\pi}{\left|\ln\frac{4\Lambda^2}{m_G^2}\right|}}, \tag{53}$$

$$\gamma_R\gamma_L \to \gamma_R\gamma_L: \quad c_\gamma \lesssim \sqrt{\frac{4\pi}{\left|\frac{11}{6} - \ln\frac{4\Lambda^2}{m_G^2}\right|}}. \tag{54}$$

In Fig. 4, we make plots for these unitarity bounds, which are set on the coupling c_γ as a function of the spin-2 particle mass m_G with a fixed cutoff scale $\Lambda = 1$ TeV. It is clear that the constraint from the channel $\gamma_R\gamma_R \to \gamma_R\gamma_R$ is much stronger than that from $\gamma_R\gamma_L \to \gamma_R\gamma_L$ for $m_G > 100$ GeV. Hence, we will apply the upper limit from $\gamma_R\gamma_R \to \gamma_R\gamma_R$ as our unitarity bound in the following numerical analysis.

4 Numerical studies

In this section, we study the constraints on the model parameter space by exploiting the unitarity bounds in Eqs. (37) and (53), which sets upper limits on the massive spin-2 particle couplings c_ℓ and c_γ. Note that the spin-2 particle model in Ref. [27] has been proposed to explain the long-standing lepton $g-2$ anomaly. Currently, the most precise value of the muon $g-2$ is provided by the combined data from

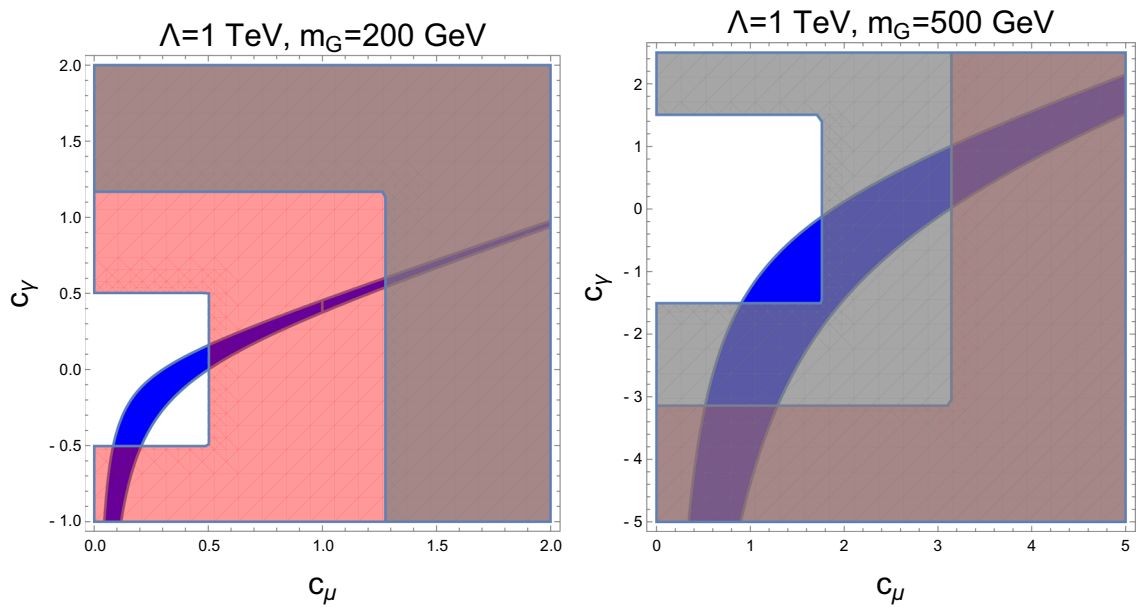

Fig. 5 The parameter space in the c_ℓ-c_γ plane for the cutoff scale fixed at $\Lambda = 1$ TeV and the spin-2 particle mass at $m_G = 200$ GeV (left panel) and 500 GeV (right panel). The blue shaded region shows the parameter space that can explain the Δa_μ anomalies in 2σ range, while the areas colored in red and gray are excluded by the theoretical constraints from perturbativity and unitarity, respectively

Brookhaven and Fermilab, which deviates the SM predictions by 4.25 σ CL. In the following discussion, we will only focus on the muon $g-2$ anomaly so that c_ℓ is taken to be c_μ.

In Fig. 5, the parameter spaces explaining the Muon $(g-2)_\mu$ data at 2σ CL are plotted as the blue shaded region in the c_ℓ–c_γ plane, where the cutoff scale is fixed to be $\Lambda = 1$ TeV and the massive graviton mass to be $m_G = 200$ GeV (left panel) and 500 GeV (right panel). In the same plots, we also lay out the constraints of the perturbativity and unitarity, and the excluded regions are colored in red and gray, respectively. As a result, it is seen from Fig. 5 that, in spite of the strong theoretical perturbativity and unitarity bounds, there is still a substantial portion of parameter space in both plots to explain the Δa_μ discrepancies. Furthermore, the comparison of the two plots in Fig. 5 indicates that, as the mass of G increases, the unitarity bounds becomes more and more important than the perturbativity ones in limiting the parameter space. Especially, when $m_G = 500$ GeV, the unitarity bounds dominate the theoretical constraint, and shrink the muon $(g-2)$ preferred region to be in a small corner with $1 < c_\ell < 2$ and $-1.5 < c_\gamma < 0$.

We can also show the relevant parameter space in the m_G–c_ℓ plane as in Fig. 6, when the cutoff scale is still fixed to be $\Lambda = 1$ TeV and the photon-G coupling is chosen as $c_\gamma = 0.5$, 0.3, 0, and -1, respectively. From these plots, it is clear that the unitarity bounds give the stronger constraint than the perturbativity ones in the large spin-2 mass regions. Remarkably, when $c_\gamma \gtrsim 0.5$, the muon $g-2$ signal regions with large m_G values which were open under the perturbativity constraints are now ruled out by the unitarity bounds. However, as the photon-G coupling c_γ decreases, more parameter spaces are now allowed by the unitarity. In one special case with $c_\gamma = 0$ where the Barr-Zee-type diagrams [66,67] give a vanishing contribution to the lepton $g-2$, it is shown in the lower-left panel that the perturbative requirement does not constrain the muon $g-2$ preferred region at all, while the spin-2 particle mass is limited to be below 500 GeV by perturbative unitarity. When c_γ further drops to take negative values, more allowed parameter regions now open with m_G extending to even larger values beyond 500 GeV, as displayed in the lower-right panel.

5 Conclusions and discussions

In Ref. [27], we explain the long-standing discrepancy between the experimental measurements and the SM prediction of the muon $g-2$ in terms of a new massive spin-2 particle, which can be easily derived in the generalized RS models. Note that we have only considered the perturbativity constraints in Ref. [27] on the model parameter space. In the present paper, we have further investigated unitarity bounds on this spin-2 particle model. We have obtained the bounds by computing the s-wave projected amplitudes for two-body elastic scatterings of charged leptons and photons in the high-energy limit for all possible initial and final helicity states. As a result, we have found that the most stringent

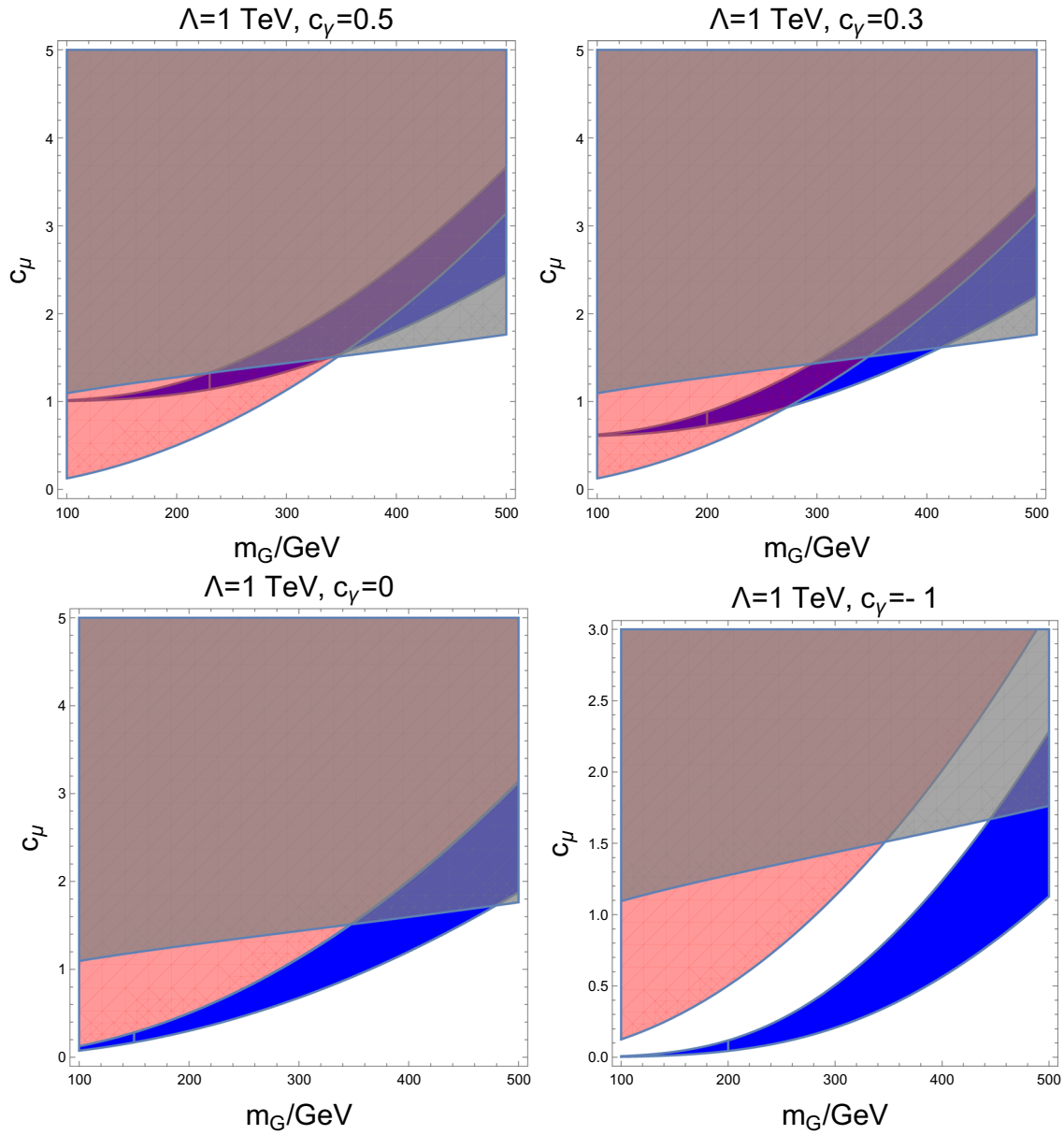

Fig. 6 The parameter space in the m_G-c_l plane with $\Lambda = 1$ TeV and $c_\gamma = 0.5$ (top-left panel), 0.3 (top-right panel), 0 (bottom-left panel), and -1 (bottom-right panel). The color coding is the same as that in Fig. 5

constraints on the lepton-G coupling c_ℓ and on the photon-G coupling c_γ are yielded via the processes $\ell_R^-\ell_R^+ \to \ell_R^-\ell_R^+$ and $\gamma_R\gamma_R \to \gamma_R\gamma_R$, respectively. We have numerically applied the obtained unitarity bounds to the spin-2 particle interpretation of the muon $g-2$ anomaly. It turns out that the tree-level S-matrix unitarity gives useful constraints on the muon $g-2$ preferred parameter regions, which is complementary to the perturbativity. In particular, it is seen that the unitarity bounds give the strongest limits on c_μ and c_γ in the large m_G region. Nevertheless, despite the stringent constraints imposed by the perturbativity and unitarity, there is still a considerable portion of parameter spaces which can explain the muon $g-2$ anomaly.

As shown in Figs. 5 and 6, the bounds from perturbativity and unitarity constrain the spin-2 particle to be relatively light with its mass $m_G \lesssim 500$ GeV. Such a light particle has already been tested by the existing collider searches, such as LEP-II and LHC. LEP-II is an electron-positron collider which has probed the quantum gravity models with the highest sensitivity in the channels of $\gamma\gamma$, e^+e^- and $\mu^+\mu^-$ [68–70]. If we parametrize the relevant couplings of G as $\epsilon \equiv \lambda/M_s^4$ following the conventions in Ref. [70] with $\lambda \sim \mathcal{O}(1)$, all these channels have constrained M_s to be

higher than around 1 TeV under the condition that the spin-2 particle has a universal coupling to photons and leptons. As illustrated in Fig. 7 of Ref. [27], the LEP-II constraints are so strong that most parameter space has been excluded for the model with $c_e = c_\mu = c_\ell$. However, if we relax the latter condition but assume that the G-electron coupling c_e is of $\mathcal{O}(0.1)$ and is much smaller than those for photons c_γ and for muons c_μ, then the above LEP-II data cannot give rise to any useful constraints on the model of a massive spin-2 particle, so that the parameter space keeps the same as in Figs. 5 and 6.

As for the LHC, the searches for the massive spin-2 particle G with the dilepton and diphoton channels at both ATLAS [71–73] and CMS [74–76] have placed stringent limits on the G-lepton and G-photon couplings. In particular, In the case of the RS model with a universal coupling to all SM particles, the lower limits on the cutoff scale, as derived from the $\ell\ell$ and $\gamma\gamma$ channels, were found to be around $\Lambda \sim \mathcal{O}(100\,\text{TeV})$ [42] for $m_G \lesssim 1$ TeV and $c_{\text{SM}} \sim 1$, which is so strong that the explanation of the muon $g-2$ anomaly has been excluded in this model. Nevertheless, this conclusion cannot hold for generalized RS models featuring non-universal SM particle couplings. Note that the constraints at the LHC are placed on the upper limits on the massive graviton production cross section times the branching fractions for these two channels. Concretely, Ref. [73] presented the search by ATLAS for the diphoton channel, with the best constraint as $\sigma(pp \to G) \times \mathcal{B}(G \to \gamma\gamma) \lesssim 2$ fb for $m_G = 500$ GeV as shown in the right plot of Fig. 5, while CMS in Ref. [76] provided the most stringent upper limit on the dimuon final state as $\sigma(pp \to G) \times \mathcal{B}(G \to \mu^+\mu^-) \lesssim 1$ fb for $m_G = 500$ GeV as shown in the upper right plot of Fig. 3. Both constraints are given at the 95% confident level. But, when the massive graviton couplings to gluons and top quarks are $c_{g,t} \sim \mathcal{O}(1)$ for $\Lambda = 1$ TeV, the constraints from the above two channels are so strong that the muon $g-2$ preferred parameter space of the massive graviton model has been excluded. The only way out is to tune c_g and c_t to be very small, so that the production of the massive graviton G is severely suppressed and the LHC constraints can be avoided. Even in the latter case, this massive graviton can still be produced at the LHC by the photon fusion [77,78] due to the large G-photon coupling. However, a further analysis of constraints from the photon fusion process is beyond the scope of the present paper, and we would like to leave it for a future work.

Acknowledgements This work is supported in part by the National Key Research and Development Program of China (Grant No. 2021 YFC2203003 and No. 2020YFC2201501), the National Natural Science Foundation of China (NSFC) (Grant No. 12005254 and No. 12147103), and the China Postdoctoral Science Foundation (Grant No. 2023M740878).

Data Availability Statement This manuscript has no associated data or the data will not be deposited. [Authors' comment: This work is just a theoretical one and we do not have any new data to provide.]

Code availability My manuscript has no associated code/software. [Author's comment: Code/Software sharing not applicable to this article as no code/software was generated or analysed during the current study.]

Funded by SCOAP[3].

References

1. R.L. Workman (Particle Data Group), PTEP **2022**, 083C01 (2022)
2. G.W. Bennett et al. (Muon g-2 Collaboration), Phys. Rev. D **73**, 072003 (2006). https://doi.org/10.1103/PhysRevD.73.072003. arXiv:hep-ex/0602035
3. B. Abi et al. (Muon g-2 Collaboration), Phys. Rev. Lett. **126**(14), 141801 (2021). https://doi.org/10.1103/PhysRevLett.126.141801. arXiv:2104.03281 [hep-ex]
4. T. Aoyama, M. Hayakawa, T. Kinoshita, M. Nio, Phys. Rev. Lett. **109**, 111808 (2012). https://doi.org/10.1103/PhysRevLett.109.111808. arXiv:1205.5370 [hep-ph]
5. T. Aoyama, T. Kinoshita, M. Nio, Atoms **7**(1), 28 (2019). https://doi.org/10.3390/atoms7010028
6. A. Czarnecki, W.J. Marciano, A. Vainshtein, Phys. Rev. D **67**, 073006 (2003). https://doi.org/10.1103/PhysRevD.67.073006. arXiv:hep-ph/0212229. [Erratum: Phys. Rev. D **73**, 119901 (2006)]
7. C. Gnendiger, D. Stöckinger, H. Stöckinger-Kim, Phys. Rev. D **88**, 053005 (2013). https://doi.org/10.1103/PhysRevD.88.053005. arXiv:1306.5546 [hep-ph]
8. M. Davier, A. Hoecker, B. Malaescu, Z. Zhang, Eur. Phys. J. C **77**(12), 827 (2017). https://doi.org/10.1140/epjc/s10052-017-5161-6. arXiv:1706.09436 [hep-ph]
9. A. Keshavarzi, D. Nomura, T. Teubner, Phys. Rev. D **97**(11), 114025 (2018). https://doi.org/10.1103/PhysRevD.97.114025. arXiv:1802.02995 [hep-ph]
10. G. Colangelo, M. Hoferichter, P. Stoffer, JHEP **02**, 006 (2019). https://doi.org/10.1007/JHEP02(2019)006. arXiv:1810.00007 [hep-ph]
11. M. Hoferichter, B.L. Hoid, B. Kubis, JHEP **08**, 137 (2019). https://doi.org/10.1007/JHEP08(2019)137. arXiv:1907.01556 [hep-ph]
12. M. Davier, A. Hoecker, B. Malaescu, Z. Zhang, Eur. Phys. J. C **80**(3), 241 (2020). https://doi.org/10.1140/epjc/s10052-020-7792-2. arXiv:1908.00921 [hep-ph]. [Erratum: Eur. Phys. J. C **80**(5), 410 (2020)]
13. A. Keshavarzi, D. Nomura, T. Teubner, Phys. Rev. D **101**(1), 014029 (2020). https://doi.org/10.1103/PhysRevD.101.014029. arXiv:1911.00367 [hep-ph]

14. A. Kurz, T. Liu, P. Marquard, M. Steinhauser, Phys. Lett. B **734**, 144–147 (2014). https://doi.org/10.1016/j.physletb.2014.05.043. arXiv:1403.6400 [hep-ph]
15. K. Melnikov, A. Vainshtein, Phys. Rev. D **70**, 113006 (2004). https://doi.org/10.1103/PhysRevD.70.113006. arXiv:hep-ph/0312226
16. P. Masjuan, P. Sanchez-Puertas, Phys. Rev. D **95**(5), 054026 (2017). https://doi.org/10.1103/PhysRevD.95.054026. arXiv:1701.05829 [hep-ph]
17. G. Colangelo, M. Hoferichter, M. Procura, P. Stoffer, JHEP **04**, 161 (2017). https://doi.org/10.1007/JHEP04(2017)161. arXiv:1702.07347 [hep-ph]
18. M. Hoferichter, B.L. Hoid, B. Kubis, S. Leupold, S.P. Schneider, JHEP **10**, 141 (2018). https://doi.org/10.1007/JHEP10(2018)141. arXiv:1808.04823 [hep-ph]
19. A. Gérardin, H.B. Meyer, A. Nyffeler, Phys. Rev. D **100**(3), 034520 (2019). https://doi.org/10.1103/PhysRevD.100.034520. arXiv:1903.09471 [hep-lat]
20. J. Bijnens, N. Hermansson-Truedsson, A. Rodríguez-Sánchez, Phys. Lett. B **798**, 134994 (2019). https://doi.org/10.1016/j.physletb.2019.134994. arXiv:1908.03331 [hep-ph]
21. G. Colangelo, F. Hagelstein, M. Hoferichter, L. Laub, P. Stoffer, JHEP **03**, 101 (2020). https://doi.org/10.1007/JHEP03(2020)101. arXiv:1910.13432 [hep-ph]
22. T. Blum, N. Christ, M. Hayakawa, T. Izubuchi, L. Jin, C. Jung, C. Lehner, Phys. Rev. Lett. **124**(13), 132002 (2020). https://doi.org/10.1103/PhysRevLett.124.132002. arXiv:1911.08123 [hep-lat]
23. G. Colangelo, M. Hoferichter, A. Nyffeler, M. Passera, P. Stoffer, Phys. Lett. B **735**, 90–91 (2014). https://doi.org/10.1016/j.physletb.2014.06.012. arXiv:1403.7512 [hep-ph]
24. E.H. Chao, R.J. Hudspith, A. Gérardin, J.R. Green, H.B. Meyer, K. Ottnad, Eur. Phys. J. C **81**(7), 651 (2021). https://doi.org/10.1140/epjc/s10052-021-09455-4. arXiv:2104.02632 [hep-lat]
25. T. Aoyama et al., Phys. Rep. **887**, 1–166 (2020). https://doi.org/10.1016/j.physrep.2020.07.006. arXiv:2006.04822 [hep-ph]
26. P. Athron, C. Balázs, D.H.J. Jacob, W. Kotlarski, D. Stöckinger, H. Stöckinger-Kim, JHEP **09**, 080 (2021). https://doi.org/10.1007/JHEP09(2021)080. arXiv:2104.03691 [hep-ph]
27. D. Huang, C.Q. Geng, J. Wu, Phys. Rev. D **107**(3), 035008 (2023). https://doi.org/10.1103/PhysRevD.107.035008. arXiv:2207.13421 [hep-ph]
28. L. Randall, R. Sundrum, Phys. Rev. Lett. **83**, 3370–3373 (1999). https://doi.org/10.1103/PhysRevLett.83.3370. arXiv:hep-ph/9905221
29. H. Davoudiasl, J.L. Hewett, T.G. Rizzo, Phys. Lett. B **473**, 43–49 (2000). https://doi.org/10.1016/S0370-2693(99)01430-6. arXiv:hep-ph/9911262
30. A. Pomarol, Phys. Lett. B **486**, 153–157 (2000). https://doi.org/10.1016/S0370-2693(00)00737-1. arXiv:hep-ph/9911294
31. S. Chang, J. Hisano, H. Nakano, N. Okada, M. Yamaguchi, Phys. Rev. D **62**, 084025 (2000). https://doi.org/10.1103/PhysRevD.62.084025. arXiv:hep-ph/9912498
32. H. Davoudiasl, J.L. Hewett, T.G. Rizzo, Phys. Rev. D **63**, 075004 (2001). https://doi.org/10.1103/PhysRevD.63.075004. arXiv:hep-ph/0006041
33. B. Batell, T. Gherghetta, Phys. Rev. D **73**, 045016 (2006). https://doi.org/10.1103/PhysRevD.73.045016. arXiv:hep-ph/0512356
34. B. Batell, T. Gherghetta, Phys. Rev. D **75**, 025022 (2007). https://doi.org/10.1103/PhysRevD.75.025022. arXiv:hep-th/0611305
35. R. Fok, C. Guimaraes, R. Lewis, V. Sanz, JHEP **12**, 062 (2012). https://doi.org/10.1007/JHEP12(2012)062. arXiv:1203.2917 [hep-ph]
36. H.M. Lee, M. Park, V. Sanz, Eur. Phys. J. C **74**, 2715 (2014). https://doi.org/10.1140/epjc/s10052-014-2715-8. arXiv:1306.4107 [hep-ph]
37. C. Han, H.M. Lee, M. Park, V. Sanz, Phys. Lett. B **755**, 371–379 (2016). https://doi.org/10.1016/j.physletb.2016.02.040. arXiv:1512.06376 [hep-ph]
38. C.Q. Geng, D. Huang, Phys. Rev. D **93**(11), 115032 (2016). https://doi.org/10.1103/PhysRevD.93.115032. arXiv:1601.07385 [hep-ph]
39. A. Falkowski, J.F. Kamenik, Phys. Rev. D **94**(1), 015008 (2016). https://doi.org/10.1103/PhysRevD.94.015008. arXiv:1603.06980 [hep-ph]
40. B.M. Dillon, V. Sanz, Phys. Rev. D **96**(3), 035008 (2017). https://doi.org/10.1103/PhysRevD.96.035008. arXiv:1603.09550 [hep-ph]
41. B.M. Dillon, C. Han, H.M. Lee, M. Park, Int. J. Mod. Phys. A **32**(33), 1745006 (2017). https://doi.org/10.1142/S0217751X17450063. arXiv:1606.07171 [hep-ph]
42. S. Kraml, U. Laa, K. Mawatari, K. Yamashita, Eur. Phys. J. C **77**(5), 326 (2017). https://doi.org/10.1140/epjc/s10052-017-4871-0. arXiv:1701.07008 [hep-ph]
43. C.Q. Geng, D. Huang, K. Yamashita, JHEP **10**, 046 (2018). https://doi.org/10.1007/JHEP10(2018)046. arXiv:1807.09643 [hep-ph]
44. A. Goyal, R. Islam, M. Kumar, JHEP **10**, 050 (2019). https://doi.org/10.1007/JHEP10(2019)050. arXiv:1905.10583 [hep-ph]
45. Y.L. Wu, Int. J. Mod. Phys. A **18**, 5363–5420 (2003). https://doi.org/10.1142/S0217751X03015222. arXiv:hep-th/0209021
46. Y.L. Wu, Mod. Phys. Lett. A **19**, 2191–2204 (2004). https://doi.org/10.1142/S0217732304015361. arXiv:hep-th/0311082
47. M. Gell-Mann, M.L. Goldberger, N.M. Kroll, F.E. Low, Phys. Rev. **179**, 1518–1527 (1969). https://doi.org/10.1103/PhysRev.179.1518
48. S. Weinberg, Phys. Rev. Lett. **27**, 1688–1691 (1971). https://doi.org/10.1103/PhysRevLett.27.1688
49. B.W. Lee, C. Quigg, H.B. Thacker, Phys. Rev. Lett. **38**, 883–885 (1977). https://doi.org/10.1103/PhysRevLett.38.883
50. B.W. Lee, C. Quigg, H.B. Thacker, Phys. Rev. D **16**, 1519 (1977). https://doi.org/10.1103/PhysRevD.16.1519
51. L. Durand, J.M. Johnson, J.L. Lopez, Phys. Rev. Lett. **64**, 1215 (1990). https://doi.org/10.1103/PhysRevLett.64.1215
52. S.L. Glashow, S. Weinberg, Phys. Rev. D **15**, 1958 (1977). https://doi.org/10.1103/PhysRevD.15.1958
53. H. Huffel, G. Pocsik, Z. Phys. C **8**, 13 (1981). https://doi.org/10.1007/BF01429824
54. J. Maalampi, J. Sirkka, I. Vilja, Phys. Lett. B **265**, 371–376 (1991). https://doi.org/10.1016/0370-2693(91)90068-2
55. S. Kanemura, T. Kubota, E. Takasugi, Phys. Lett. B **313**, 155–160 (1993). https://doi.org/10.1016/0370-2693(93)91205-2. arXiv:hep-ph/9303263
56. A.G. Akeroyd, A. Arhrib, E.M. Naimi, Phys. Lett. B **490**, 119–124 (2000). https://doi.org/10.1016/S0370-2693(00)00962-X. arXiv:hep-ph/0006035
57. D. Das, I. Saha, Phys. Rev. D **91**(9), 095024 (2015). https://doi.org/10.1103/PhysRevD.91.095024. arXiv:1503.02135 [hep-ph]
58. S. Kanemura, K. Yagyu, Phys. Lett. B **751**, 289–296 (2015). https://doi.org/10.1016/j.physletb.2015.10.047. arXiv:1509.06060 [hep-ph]
59. M.D. Goodsell, F. Staub, Eur. Phys. J. C **78**(8), 649 (2018). https://doi.org/10.1140/epjc/s10052-018-6127-z. arXiv:1805.07306 [hep-ph]
60. T. Appelquist, M.S. Chanowitz, Phys. Rev. Lett. **59**, 2405 (1987). https://doi.org/10.1103/PhysRevLett.59.2405. [Erratum: Phys. Rev. Lett. **60**, 1589 (1988)]
61. M. Chaichian, J. Fischer, Nucl. Phys. B **303**, 557–568 (1988). https://doi.org/10.1016/0550-3213(88)90394-X
62. I. Banta, T. Cohen, N. Craig, X. Lu, D. Sutherland, JHEP **02**, 029 (2022). https://doi.org/10.1007/JHEP02(2022)029. arXiv:2110.02967 [hep-ph]

63. T. Han, J.D. Lykken, R.J. Zhang, Phys. Rev. D **59**, 105006 (1999). https://doi.org/10.1103/PhysRevD.59.105006. arXiv:hep-ph/9811350
64. M.L. Graesser, Phys. Rev. D **61**, 074019 (2000). https://doi.org/10.1103/PhysRevD.61.074019. arXiv:hep-ph/9902310
65. M. Nebot, J.F. Oliver, D. Palao, A. Santamaria, Phys. Rev. D **77**, 093013 (2008). https://doi.org/10.1103/PhysRevD.77.093013. arXiv:0711.0483 [hep-ph]
66. J.D. Bjorken, S. Weinberg, Phys. Rev. Lett. **38**, 622 (1977). https://doi.org/10.1103/PhysRevLett.38.622
67. S.M. Barr, A. Zee, Phys. Rev. Lett. **65**, 21–24 (1990). https://doi.org/10.1103/PhysRevLett.65.21. [Erratum: Phys. Rev. Lett. **65**, 2920 (1990)]
68. J. Abdallah et al. (DELPHI Collaboration), Eur. Phys. J. C **45**, 589–632 (2006). https://doi.org/10.1140/epjc/s2005-02461-0. arXiv:hep-ex/0512012
69. J. Alcaraz et al. (ALEPH, DELPHI, L3, OPAL and LEP Electroweak Working Group), arXiv:hep-ex/0612034
70. S. Schael et al. (ALEPH, DELPHI, L3, OPAL and LEP Electroweak Working Group), Phys. Rep. **532**, 119–244 (2013). https://doi.org/10.1016/j.physrep.2013.07.004. arXiv:1302.3415 [hep-ex]
71. G. Aad et al. (ATLAS Collaboration), Phys. Lett. B **796**, 68–87 (2019). https://doi.org/10.1016/j.physletb.2019.07.016. arXiv:1903.06248 [hep-ex]
72. Y. Wang (ATLAS Collaboration), PoS **ICHEP2020**, 109 (2021). https://doi.org/10.22323/1.390.0109
73. G. Aad et al. (ATLAS), Phys. Lett. B **822**, 136651 (2021). https://doi.org/10.1016/j.physletb.2021.136651. arXiv:2102.13405 [hep-ex]
74. A.M. Sirunyan et al. (CMS Collaboration), JHEP **06**, 120 (2018). https://doi.org/10.1007/JHEP06(2018)120. arXiv:1803.06292 [hep-ex]
75. A.M. Sirunyan et al. (CMS Collaboration), Phys. Rev. D **98**(9), 092001 (2018). https://doi.org/10.1103/PhysRevD.98.092001. arXiv:1809.00327 [hep-ex]
76. A.M. Sirunyan et al. (CMS), JHEP **07**, 208 (2021). https://doi.org/10.1007/JHEP07(2021)208. arXiv:2103.02708 [hep-ex]
77. A. Tumasyan et al. (CMS and TOTEM), arXiv:2311.02725 [hep-ex]
78. D. d'Enterria, M.A. Tamlihat, L. Schoeffel, H.S. Shao, Y. Tayalati, Phys. Lett. B **846**, 138237 (2023). https://doi.org/10.1016/j.physletb.2023.138237. arXiv:2306.15558 [hep-ph]